



Article

The Evolution of the IR and Raman Spectra When the Symmetry Reduces—The Case of the LaCoO₃ Perovskite †

Tarek Larbi^{1,2,*}, Klaus Doll³, Michel Rerat⁴ and Roberto Dovesi⁵¹ Laboratoire de Nanomatériaux Nanotechnologie et Energie, Faculté des sciences de Tunis, Université de Tunis, El Manar, Tunis 2092, Tunisia² Université de Tunis, IPEIT, 2, Rue Jawaher Lel Nehru, Montfleury, Tunis 1089, Tunisia³ Molpro Quantum Chemistry Software, Institute for Theoretical Chemistry, University of Stuttgart, Pfaffenwaldring 55, D, 70569 Stuttgart, Germany⁴ Université de Pau et des pays de l'Adour, CNRS, IPREM UMR 5254, E2S UPPA, 64000 Pau, France⁵ Accademia Delle Scienze Di Torino, Via Accademia delle Scienze 6, 10123 Torino, Italy* Correspondence: 107tarek@yahoo.fr

† This article is dedicated to Prof. Giuseppe Zerbi in recognition of his outstanding scientific contributions to Spectroscopy.

How To Cite: Larbi, T.; Doll, K.; Rerat, M.; et al. The Evolution of the IR and Raman Spectra When the Symmetry Reduces—The Case of the LaCo₃ Perovskite. *Photochemistry and Spectroscopy* **2026**, *2*(1), 2. <https://doi.org/10.53941/ps.2026.100002>

Received: 11 July 2025

Revised: 7 August 2025

Accepted: 8 August 2025

Published: 20 January 2026

Abstract: The IR and Raman spectra of the LaCoO₃ perovskite (the formal occupancy on Co is d⁶, low spin, t_{2g}⁶) are computed by imposing space groups (SG) of decreasing symmetry, from the cubic (SG Pm-3m, N. 221, and Fm-3m, N. 225), to the tetragonal (SG 140), rhombohedral (SG 167) and orthorhombic (SG 62) ones. The total energy differences between these structures, computed at the quantum mechanical level by using an all electron Gaussian type basis set and the *full range* hybrid B3LYP functional, is extremely small: 0.2 mE_h between SG 167 and SG 62, 1.2 mE_h between SG 140 and SG 62, and 4.5 mE_h between the most stable structure and the cubic, ideal aristotype. These minor differences indicate that the experimentally proposed SG might be one of the (many) possible alternatives. The IR and Raman spectra are very rarely used for the identification of the symmetry of the perovskites at different temperatures. Here we investigate the evolution of the two spectra (IR and Raman) through the various competing space groups, exploring the possibility that they might be used for the identification of the low temperature structure (SG and position of the atoms) of the investigated compounds, and of perovskites in particular.

Keywords: LaCoO₃ perovskite; IR and Raman spectra; evolution of the spectra with symmetry; cubic; tetragonal; orthorhombic and rhombohedral space groups

1. Introduction

The ideal structure of ABX₃ perovskites is cubic. There are, however, at least three mechanisms which force a symmetry lowering, and, possibly, an increase of the size of the unit cell, from 1 to 2 or 4 formula units (f.u.):

- I. The Jahn-Teller splitting of the t_{2g} or e_g sub-shells of B, when they are partially filled and B is a first row transition metal (TM).
- II. The displacement (say vertically) of the TM at the center of the octahedron, as a consequence of the overlap of its d orbitals with the p orbitals of the ligand (usually the second or third TM row atoms are involved, for which the d shell is more diffuse than in the first row): the inversion center is lost, and this reduces the total energy (the symmetric position of B turns out to be a maximum).
- III. The BX₆ octahedra rotate with respect to one, two or three cartesian directions [1,2]. This is actually what happens, for example, in KMnF₃, whose most stable space group (SG) is Pbnm (N. 62), and in KVF₃, whose most stable SG is I4/mcm (N. 140) (see References [3,4]).



Copyright: © 2026 by the authors. This is an open access article under the terms and conditions of the Creative Commons Attribution (CC BY) license (<https://creativecommons.org/licenses/by/4.0/>).

Publisher's Note: Scilight stays neutral with regard to jurisdictional claims in published maps and institutional affiliations.

A tolerance factor [5], t , defined in terms of the ionic radii [6] of A, B and X:

$$t = \frac{r_X + r_A}{\sqrt{2}(r_X + r_B)} \quad (1)$$

is usually used for determining the behavior of ABX_3 . The above formula is obviously empirical, and based on ionic radii obtained by best fit from sets of geometrical data, under the hypothesis of the transferability from system to system. For examples and discussions on the relationship between t and the space group, see the recent paper by Dubrovin et al. in reference [7].

In many cases, however, the deformation of the unit cell can be so large that the classification with respect to the three mechanisms described above becomes inaccurate or impossible: if the deformation of the BX_6 octahedra is large, the geometry modification cannot be described in terms of a simple parameter, like a rotation (mechanism III) of the octahedron, or the displacement of the B cation from the center of the octahedron, which remains essentially regular (mechanism II). In the present case, the situation is the following. Mechanisms I and II can be excluded because the configuration of the Co d shell is $(t2g)^6$ (I), and because Co belongs to the first transition metal row. As regards mechanism III, the tolerance t factor for $LaCoO_3$ is very close to one, when the Shannon⁶ ionic radii are used, so that a relatively small deformation of the octahedron, if any, is to be expected.

The available experimental determinations of the structure along the series $LaBO_3$ [8–20], with B from Sc to Cu, suggest that most of the systems at the beginning of the series (Sc, Ti, Cr, Mn, Fe, but not V, attributed to a monoclinic SG) belong to SG Pbnm, N. 62, orthorhombic, whereas the last three members (Co, Ni, Cu) are attributed to SG R-3c, N. 167 (although in the Cu case also a second attribution has been proposed, to SG I4/m, N. 87).

The experimental papers are in many cases very old (when the X-ray or neutron scattering techniques were not so accurate as nowadays), spanning nearly 50 years [8,9]. Many other technical details (for example the degree of purity of the sample, its dimension, its crystallinity) might certainly influence the attribution of the structure to one SG rather than to another. We remind that the attribution is based on statistical arguments, selecting in general the SG with lowest R factor (corresponding to best agreement) and higher symmetry (a compromise is necessary between the two variables). We also remind that in most of the quantum mechanical simulations of the properties of the perovskites, calculations are performed using the SG proposed in the literature, without any cross check with other possible alternative structures.

In the present manuscript, we decided to tackle the problem from two points of view:

- (a) we investigate other possible SGs, which might be more stable, or slightly less stable than the one proposed by experimentalists.
- (b) we explore the differences in the IR and Raman spectra of these competitive structures. It might happen that structures with very similar total energy are characterized by quite different IR and Raman spectra, that might be used for discriminating between the proposed SGs.

In the present study, devoted to $LaCoO_3$, first we tackle point (a), comparing the total energy and the equilibrium geometry when different SGs are imposed: cubic Pm-3m and Fm-3m, tetragonal I4/mcm, rhombohedral R-3c, orthorhombic Pbnm. As the total energy of these structures is relatively similar, we will generate then the IR and RAMAN spectra (point (b)), with the aim of:

- I. Exploring if they are stable structures (possible imaginary wavenumbers, see below)
- II. Verifying whether the similar total energy corresponds to a similar spectrum, or, vice versa, to spectra with quite different features.

The paper is structured as follows:

In section II the computational conditions are defined. In section III the IR and Raman spectra of the FM solutions are presented for various SGs. The conclusions follow in section IV.

2. Computational Details

The closed shell solutions for the various phases of $LaCoO_3$ have been obtained at the B3LYP [21,22] level by using an *all electron* Gaussian type basis set and the CRYSTAL code [23,24]. The triple zeta type 9-763311(631)G, 8-6411(51d)G and 8-411(1)G contractions, consisting of 1s, 6sp and 3d shells (40 atomic orbitals, AOs) for La, of 1s, 4sp and 2d shells (27 AOs), for Co, and of 1s, 3sp and 1d shells (18 AOs) for oxygen, for a total of 121 AOs per formula unit, have been used. The Coulomb and Hartree-Fock exchange series are controlled by five parameters [23] that were set to $T1 = T2 = T3 = T4$ and $T5 = 2 \times T1$, with $T1 = 10$ (for a complete description of the role of these parameters see also Refs. [25,26]; these values are required for an accurate evaluation of the small differences between the various phases of the system, ranging between 10^{-3} and 10^{-5} E_h). As regards the DFT exchange-correlation contribution to the Fock matrix, it was evaluated by numerical integration over the unit cell

volume. Radial and angular points for the integration grid were generated through a Gauss-Legendre radial quadrature and Lebedev two-dimensional angular point distributions. In the present work, a pruned grid with 99 radial and 1454 angular points was used (see XXLGRID keyword in the CRYSTAL manual [23]). The integration accuracy can be estimated by the error in the electronic charge of the unit cell: 432.000030 electrons, to be compared to 432.000000 electrons of the unit cell of LaCoO₃ with 4 formula units in Pbnm (62). All calculations have been performed by using a supercell of the primitive cell, containing one, two or four magnetic centers.

A. Vibrational frequencies, infrared and Raman spectra

Vibrational frequencies and related properties have been available in CRYSTAL for more than 15 years (CRYSTAL06) [27]. Frequencies at the Γ point are obtained within the harmonic approximation by diagonalizing the mass-weighted Hessian matrix, W , whose elements are defined as [28–30]:

$$W_{\alpha i, \beta j}^{\Gamma} = \frac{H_{\alpha i, \beta j}^0}{\sqrt{M_{\epsilon} M_{\beta}}} \quad \text{with} \quad H_{\alpha i, \beta j}^0 = \frac{\partial^2 E}{\partial u_{\alpha i}^0 \partial u_{\beta j}^0} \quad (2)$$

where M_{α} and M_{β} are the masses of the atoms associated with the i and j Cartesian coordinates of atoms α and β . Energy first derivatives with respect to the atomic positions, $g_{\alpha j} = \partial E / \partial u_{\alpha j}$, are calculated analytically for all $u_{\alpha j}$ coordinates (E is the total energy, $u_{\alpha j}$ is the displacement coordinate with respect to equilibrium). Second derivatives at $u = 0$ are calculated numerically using a single displacement along each coordinate ($N = 2$, the central point and a point on the positive direction of the coordinate):

$$\frac{\partial g_{\alpha j}}{\partial u_{\beta i}} = \frac{g_{\alpha j}(0, \dots, u_{\beta i}, \dots)}{u_{\beta i}} \quad (3)$$

or averaging two displacements ($N = 3$):

$$\frac{\partial g_{\alpha j}}{\partial u_{\beta i}} \approx \frac{g_{\alpha j}(0, \dots, u_{\beta i}, \dots) - g_{\alpha j}(0, \dots, -u_{\beta i}, \dots)}{2u_{\beta i}} \quad (4)$$

The default value for N is 2; this corresponds to computing $3N-3$ displacements, for each of which a SCF + gradient (G) calculation is performed. The default value for the displacement (0.003 Å) is used. Infrared (IR) and Raman intensities are evaluated analytically through the CPHF scheme [29–33]. The IR and Raman spectra can then easily be generated.

3. Results

In a previous paper [34], (see also Ref. [35]) by some of the present authors, it has been shown that the most stable structure of LaCoO₃ belongs to the R-3c space group, as suggested by experiments [15,16]. Table 1 shows however that two alternative attributions are possible for the low energy space group, namely Pbnm, $N. 62$, and I4/mcm, $N. 140$, which differ in energy from R-3c by an extremely small amount, 0.2 mE_h (about 63 K) the former, and 1.1 mE_h the latter. But also the perfect cubic solution is not far, just 4.5 mE_h above the R-3c energy.

Table 1. Total energy E (in E_h), cell volume (in Å³) and band gap (in eV) of the LaCoO₃ perovskite, when the space group symmetry decreases from Pm-3m (cubic, $N. 221$) to Pbnm (orthorhombic, $N. 62$). In SG 221 the unit cell contains 1 f.u., in SG 140 and 167, 2 f.u., in SG 62 4 f.u. The energies and volumes are per f.u. ΔE (in mE_h) is the difference with respect to the total energy of SG 221. In SG 140 the octahedra are allowed to rotate with respect to one axis, in SG 62 they can rotate with respect to three axes and the d occupancy on B can flip from site to site. In SG 167 the apical angle of the octahedra can deform.

	SG	E	ΔE	V	Gap
LaCoO ₃	Pm-3m (221)	-9832.377967	0	57.182	2.33
	I4/mcm (140)	-9832.381335	-3.4	57.636	2.46
	Pbnm (62)	-9832.382245	-4.3	57.813	2.54
	R-3c	-9832.382446	-4.5	57.834	2.55

These small energy differences correspond to small differences in the cell volume, as Table 1 shows (only 0.3% between SG I4/mcm and R-3c, which increases to 1% between SG Pm-3m and R-3c). Also the geometry of the octahedron is very similar: let us consider R , the Co-O distance: in SG 221 and SG 167 the six R are equivalent, 1.926 Å (cubic) and 1.956 Å (rhombohedral). In SG 140 the six R split in 4 (equatorial), at 1.945 Å, and 2 (apical), at 1.947 Å. Finally, in SG 62 three independent R values are possible, which are however extremely similar: 1.951, 1.951, 1.953 Å. The Co-O distances differ then in the three most stable SGs at most by 0.011 Å (from 1.945 to 1.956 Å). In the following, we focus on the difference in the equilibrium geometry of SG 140, 62 and 167. In the

cubic structure, the six Co-O distances are the same. In space group 167, the compression (positive or negative) along one of the principal directions (say *c*) is the only possible deformation: the 8 triangular faces of the octahedron, which are equilateral in the perfect geometry, become isosceles, with the $\widehat{O_1O_2O_3}$ angle increasing from 60° to 61.3° (O_2 is an apical oxygen). The other possibility is exploited in SG 140 and 62: the octahedron remains essentially regular, but rotates by some amount with respect to *c* in SG 140, where $\widehat{Co_1O_1O_2}$ is 162.8° instead of 180°. In SG 62, two $\widehat{Co_1O_1O_i}$ angles can describe the rotation with respect to two orthogonal directions, and are 161.4° and 165.8°, (where Co_1 is at the center of the octahedron, and Co_i is one of its first neighbors). The extreme similarity of the solution for SG 140, 62 and 167 is confirmed by the very close values of the band gap (2.46, 2.54, 2.55 eV, respectively). Also the charge and spin densities are extremely similar.

A. The IR and Raman spectra of the cubic phase

In the Pm-3m unit cell, the 5 atoms generate 15 modes at the Γ point, organized in 5 triply degenerate peaks, four of F_{1u} and one of F_{2u} symmetry. One F_{1u} triple mode describes actually the translations, so that the vibrational reducible representation decomposes as follows:

$$\Gamma_{red}^{vib} = 3 F_{1u} + 1 F_{2u}$$

These modes are of *u* (*ungerade*) symmetry, so that they are Raman inactive (only *g* (*gerade*) modes can be Raman active). The components of the \vec{r} vector, representing the electric field, belong to the F_{1u} irreducible representation (IRREP), so that the F_{2u} modes are IR inactive. The isotopic shift (see Tables below), attributes the four triply-degenerate F_{1u} and F_{2u} modes as follows:

- (1) The modes at 143 cm^{-1} are essentially translation modes of the La cation.
- (2) The modes at 209 cm^{-1} (F_{2u} symmetry) are rocking modes; the octahedron is rotating rigidly. These modes are silent both in IR and Raman.
- (3) The modes at 282 cm^{-1} are bending movements involving the O-Co-O chain. Co and the two O atoms are moving in opposite directions, and the \widehat{OCoO} angle is changing.
- (4) The modes at 532 cm^{-1} are stretching movements: the Co-O distance is increasing and reducing.

All modes are triply degenerate: for example there are three bending modes, one along *x*, one along *y* and one along *z*. The wavenumbers are also shown in Table 2; the right column gives the shift of the modes (obtained after rediagonalizing the dynamical matrix) when the mass of La, or Co, or O, is increased by 20% in three independent calculations). As the mass increases, the wavenumbers decrease (or remain unaltered, if they are not involved at all in the mode). In the case of La, the largest shift, 5 cm^{-1} , is for the lowest wavenumber, confirming that this is the La *translation* mode. When the Co mass is increased, the largest shift (12 cm^{-1}) is for the bending mode at 282 cm^{-1} , the other shifts being much smaller (only 3 and 2 cm^{-1}). The last column shows also the shifts due to the increase of the O mass. As oxygen is the *glue* of the structure, it is deeply involved in all modes. Note however that the largest shift, 43 cm^{-1} , is for the stretching mode at 532 cm^{-1} , in which the O ions are moving back and forth.

Table 2. Wavenumbers (ν in cm^{-1}) and intensities (IR (in kmmol^{-1}) and Raman (in $\text{\AA}^4\text{amu}^{-1}$)) for SG 221. Δ is the isotopic frequency shift (in cm^{-1}) when the mass of La, Co and O is increased by 20% (in three independent calculations). The intensities (which are extensive quantities) refer to two formula units.

LaCoO ₃ Cubic Pm-3m, N 221								
N	Mode	ν	IR Intensity	Raman Intensity	Δ/Co	Δ/La	Δ/O	
4–6	F_{1u}	143	3016	-	-3	-5	-5	
7–9	F_{2u}	209	-	-	0	0	-18	
10–12	F_{1u}	282	5822	-	-12	0	-11	
13–15	F_{1u}	532	5846	-	-2	0	-43	

B. What happens when doubling the cell size from Pm-3m to Fm-3m

In order to make the comparison with the spectra of the tetragonal (SG 140) and rhombohedral (SG 167) cells, containing both 10 atoms/cell, we doubled the Pm-3m cell to its face-centered counterpart, Fm-3m, containing 10 atoms/cell. In this case the modes are 27 (three translations must be added to reach $10 \times 3 = 30$ modes). The total energy, and equilibrium geometry per f.u. are exactly the same, as they should be. At Γ , however, now we have more modes, in addition to the ones present in the Pm-3m spectrum. Of the new modes, only one is of ungerade symmetry, at 402 cm^{-1} , but essentially null intensity, so it does not appear in the spectrum. The 12 remaining new modes are gerade and then, in principle, Raman active. The Raman intensities are however

extremely low (essentially numerical noise). One of the g modes is a triply degenerate mode of F_{1g} symmetry, corresponding to an imaginary wavenumber at 177i (i = imaginary unit), that in the Table 3 is indicated as negative. This confirms that the structure, optimized with SG 225, is not a minimum: it is a saddle point. Releasing the symmetry constraints, it would fall down towards a lower energy and lower symmetry. There are two F_{2g} sets, the first of which is the symmetric counterpart of the La translation (136 vs 143 cm^{-1}), as the isotopic shift confirms (12 cm^{-1}). The second F_{2g} set is at 381 cm^{-1} (the symmetric counterpart of the F_{1u} mode at 402 cm^{-1}). The remaining modes, of E_g and A_g symmetry, are at much higher wavenumbers (642 and 783 cm^{-1}) than the highest mode in the IR spectrum.

Table 3. Wavenumbers (ν in cm^{-1}) and intensities (IR (in kmmol^{-1}) and Raman (in $\text{\AA}^4\text{amu}^{-1}$)) for SG 225. Δ is the isotopic frequency shift (in cm^{-1}) when the mass of La, Co and O is increased by 20% (in three independent calculations). The intensities (which are extensive quantities) refer to two formula units. The Raman intensities and the IR intensity of the mode at 402 cm^{-1} are however just numerical noise. They should be zero like in the Pm-3m structure, where no Raman active modes are observed.

LaCoO ₃ Cubic Fm-3m, N 225							
N	Mode	ν	IR Intensity	Raman Intensity	Δ/Co	Δ/La	Δ/O
1–3	F_{1g}	-177	-	-	0	0	15
7–9	F_{2g}	136	-	0.1223×10^{-2}	0	-12	0
10–12	F_{1u}	143	3033	-	-3	-5	-5
13–15	F_{2u}	211	-	-	0	0	-18
16–18	F_{1u}	287	5552	-	-12	0	-12
19–21	F_{2g}	381	-	0.5141×10^{-2}	-13	0	-32
22–24	F_{1u}	402	1.83	-	-21	0	0
25–27	F_{1u}	536	5895	-	-3	0	-44
28–29	E_g	642	-	0.1924×10^{-2}	0	0	-56
30–30	A_g	783	-	0.4982×10^{-3}	0	0	-68

As anticipated, the Raman intensities are essentially null, so that the Raman spectrum is not providing any additional information with respect to the IR spectrum.

C. From the cubic to the tetragonal and rhombohedral spectra

The tetragonal phase, with SG I4/mcm, differs by 3.4 mE_h from the cubic phase. We will address the question whether this difference is large enough so that it produces important modifications in the IR and Raman spectra; in particular, whether the three dominant F_{1u} peaks, corresponding to the translation of La, to the stretching and bending of the octahedron, remain the most visible features of the IR spectrum. In principle, the cubic F_{1u} modes split into one E_u and one A_{2u} mode, and the F_{2u} into E_u and B_{2u} (same for the gerade symmetries). The splitting is however a function of the nature of the mode, and of the deformation of the cell. Let us consider first the IR spectrum. We can then measure the effect of the small rotation of the octahedron on the spectrum, by looking at the difference between the E_u and the A_{2u} (or B_{2u}), and by using two indices (see Table 4): β_1 , the splitting of two peaks coming from a triply degenerate cubic level, and β_2 , the shift of the baricenter between E_u and A_{2u} with respect to F_{1u} (same for F_{2u}). The splitting of the triply degenerated modes is not huge, as Table 4 confirms: 15, 6 and 17 cm^{-1} from the low to the high wavenumbers. The β_2 values, measuring the shift of the baricenter of the $E_u + A_{2u}$ band with respect to the cubic position is quite large, +33, +55 and -14 cm^{-1} . However, looking at the spectrum in Figure 1, the three “cubic” peaks dominate also the tetragonal spectrum (see also Table 5). It should however be noticed that two additional peaks appear, at 260 and 409 cm^{-1} , both related to the rotation of the octahedron. Their intensity is competitive with the highest peaks coming from the cubic spectrum.

The description of the IR spectrum of the most stable structure, R-3c (see the full set of wavenumbers and intensities in Table 6), is very similar to the one for I4/mcm, with the extra peaks at about the same wavenumbers as in the tetragonal spectrum (257 vs 260 cm^{-1} and 425 vs 409 cm^{-1}), but with the important difference that the peak at 425 cm^{-1} is the most intense of the set of peaks. This peak might be used as a fingerprint of the R-3c structure. The I4/mcm and R-3c Raman spectra are quite different from each other, and from the Fm-3m one. However the intensities remain relatively low, confirming the difficulties of obtaining Raman spectra of these compounds.

Table 4. The wavenumbers of the modes active in the IR spectrum of the cubic cell (second column), and how they split in the tetragonal I4/mcm, rhombohedral R-3c and orthorhombic Pbnm space groups. LaCoO₃, B3LYP solution. β_1 is the amount of the splitting of the cubic, triply degenerate mode due to the reduction of symmetry. β_2 is the shift of the barycenter of the two tetragonal, rhombohedral and orthorhombic modes with respect to the cubic wavenumber.

Mode	Fm-3m		I4/mcm			R-3c				Pbnm				
	F _{1u}	E _u	A _{2u}	β_1	β_2	E _u	A _{2u}	β_1	β_2	B _{1u}	B _{2u}	B _{3u}	β_1	β_2
1	143	171	186	+15	+33	188	166	-22	+37	250	293	313	+63	+142
2	282	333	339	-6	+55	341	316	-25	+50	425	456	476	+51	+170
3	532	524	507	-17	-14	522	497	-25	-19	491	513	532	+41	-20

Table 5. Wavenumbers (ν in cm⁻¹) and intensities (IR (in kmol⁻¹) and Raman (in Å⁴amu⁻¹)) for SG 140. The red lines indicate the modes originating from the corresponding *cubic* mode. Δ is the isotopic frequency shift (in cm⁻¹) when the mass of La, Co and O is increased by 20% (in three independent calculations). The intensities (which are extensive quantities) refer to two formula units.

LaCoO ₃ Tetragonal I4/mcm, N 140							
N	Mode	ν	IR Intensity	Raman Intensity	Δ/Co	Δ/La	Δ/O
1–2	E _g	-102	-	0.6668	0	0	9
6–7	E _g	157	-	-	0	-13	0
8–8	B _{2g}	161	-	0.185	0	-14	0
9–10	E _u	171	1202	-	-4	-6	-5
11–11	A _{2u}	186	539	-	-6	-6	-3
12–12	A _{1g}	259	-	0.151	-3	0	-22
13–14	E _u	260	481	-	-1	0	-18
15–15	B _{1u}	322	-	-	-3	0	-28
16–16	A _{2u}	333	1617	-	-11	0	-18
17–18	E _u	339	993	-	-16	0	-13
19–19	A _{1u}	388	-	-	-33	0	-20
20–21	E _g	404	-	2.588	-14	0	-15
22–23	E _u	409	996	-	-5	0	-12
24–24	B _{2g}	448	-	0.4259	0	0	-39
25–25	A _{2u}	507	59	-	-1	0	-43
26–27	E _u	524	388	-	-3	0	-42
28–28	A _{2g}	598	-	-	0	0	-52
29–29	B _{1g}	599	-	0.163	0	0	-52
30–30	A _{2g}	731	-	-	0	0	-64

Table 6. Wavenumbers (ν in cm⁻¹) and intensities (IR (in kmol⁻¹) and Raman (in Å⁴amu⁻¹)) for SG 167. Δ is the isotopic frequency shift (in cm⁻¹) when the mass of La, Co and O is increased by 20% (in three independent calculations). The red lines indicate the modes originating from the corresponding *cubic* mode. The blue line shows that one extra mode (E_g) appears in between the A_{2u} and E_u modes, corresponding to the La *translation*. The intensities (which are extensive quantities) refer to two formula units.

LaCoO ₃ Trigonal R-3c, N 167							
N	Mode	ν	IR Intensity	Raman Intensity	Δ/Co	Δ/La	Δ/O
4–5	E _g	116	-	1.6	0	-3	-8
6–6	A _{2g}	145	-	-	0	-13	-0
7–7	A _{2u}	166	617	-	-4	-6	-5
8–9	E _g	183	-	30	0	-11	-3
10–11	E _u	188	910	-	-5	-6	-5
12–13	E _u	257	527	-	-4	0	-17
14	A _{1g}	278	-	43	0	0	-24
15	A _{2u}	316	1438	-	-11	0	-16
16–17	E _u	341	2174	-	-22	0	-9
18–18	A _{1u}	371	-	-	-29	0	-21
19–19	A _{2g}	383	-	-	0	0	-22
20–20	A _{1u}	419	-	-	-10	0	-25
21–22	E _u	425	2670	-	-9	0	-17
23–24	E _g	458	-	75	0	0	-4
25	A _{2u}	497	1637	-	-3	0	-4
26–27	E _u	522	1796	-	-1	0	-43
28–29	E _g	585	-	11	0	0	-5
30–30	A _{2g}	713	-	-	0	0	-62

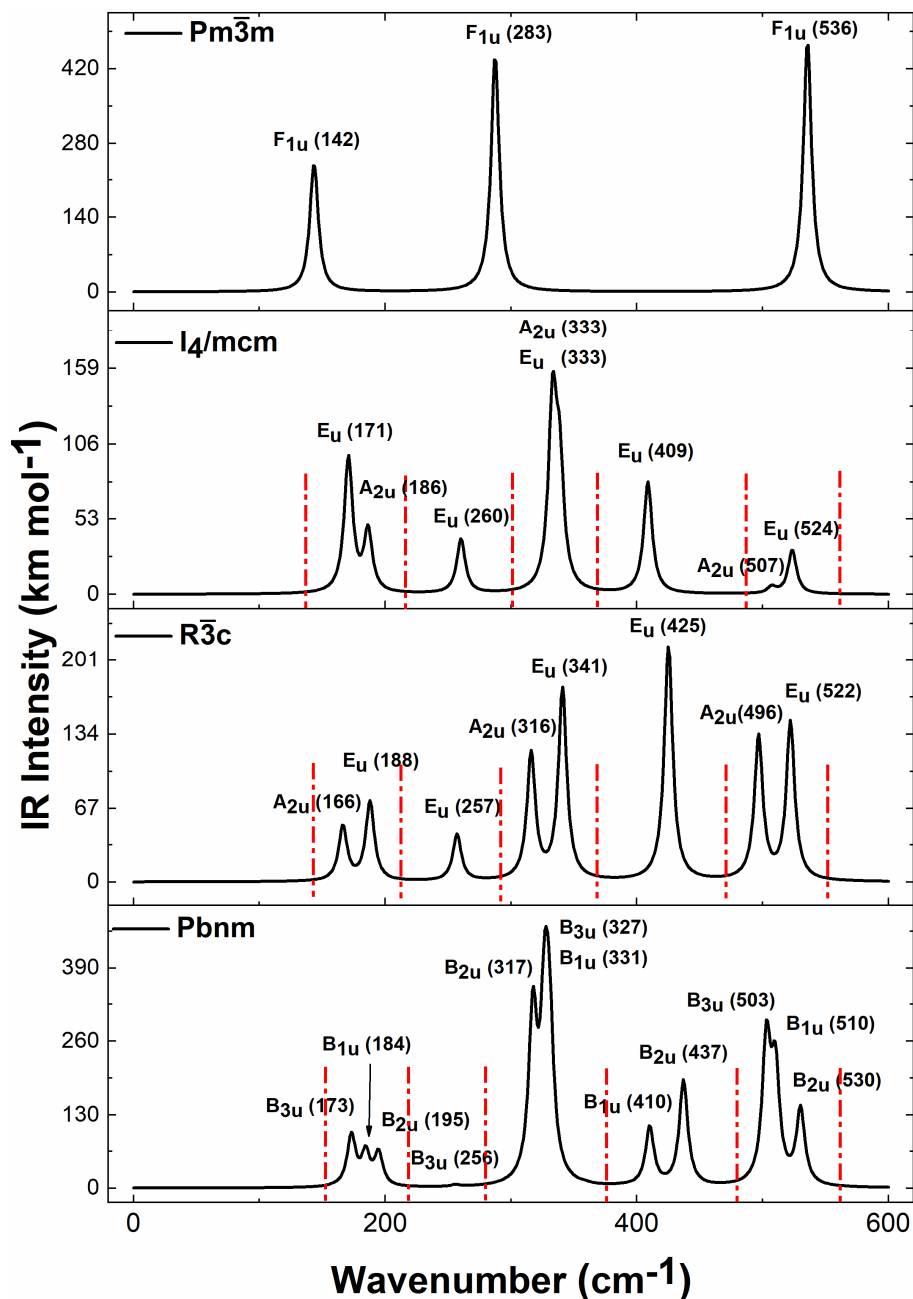


Figure 1. Infrared spectrum of LaCoO_3 obtained with four different space groups of decreasing symmetry. The wavenumber and symmetry of the most relevant peaks are shown. In the interval between two dot-dashed vertical bars (in red), are contained the modes originating from the split of the three modes present in the cubic spectrum. The wavenumber, symmetry and intensity of all the modes are given in Tables 2–6.

D. The orthorhombic spectrum

The total energy of the $Pbnm$ structure is very close to the $R\bar{3}c$ one, corresponding to the lowest energy at $T = 0$ K. Both the IR and Raman spectra are however quite different, in many respects. In the IR spectrum, the original structure of the cubic spectrum is lost to a large amount. The three main peaks split in the $I4/mcm$ and $R\bar{3}c$ SGs, but remain however well separated from each other and from the new peaks originating from the deformation. In the bottom panel of Figure 2, the separation of the B_1 , B_2 and B_3 peaks, originating from the F_{1u} cubic peaks, is larger, and mixed, to some amount, with the new peaks originating from the octahedron rotations. Also the Raman spectrum differs significantly from the ones of the higher symmetry structures. In particular, the most intense peak falls at 467 cm^{-1} , whereas the highest one is at 458 cm^{-1} for $R\bar{3}c$, and 404 cm^{-1} for $I4/mcm$. The Raman intensities, as a consequence of the reduced symmetry, are higher than for the other symmetries, as shown in Table 7.

Table 7. Wavenumbers (ν in cm^{-1}) and intensities (IR (in kmol^{-1}) and Raman (in $\text{\AA}^4\text{amu}^{-1}$)) for SG 62. Δ is the isotopic frequency shift (in cm^{-1}) when the mass of La, Co and O is increased by 20% (in three independent calculations). The red lines indicate the modes originating from the corresponding cubic mode. The blue line shows the extra modes which appear in the interval spanned by the B_1 B_2 and B_3 set originating from one of the *cubic* modes. The intensities (which are extensive quantities) refer to two formula units.

LaCoO ₃ Orthorhombic, Pbnm, N 62								
N	Mode	ν	IR Intensity	Raman Intensity	Δ/Co	Δ/La	Δ/O	
4	A _g	35	0	1.14×10^{-2}	0	-2	-1	
5	B _{2g}	60	0	5.22	0	0	-5	
6	A _u	97	0	-	0	-8	-1	
7	B _{1g}	116	0	1.39×10^{-2}	0	-10	0	
8	B _{1g}	138	0	6.25×10^{-1}	0	-8	-7	
9	B _{2u}	141	0	-	-1	-11	-1	
10	B _{3g}	158	0	5.35×10^{-1}	0	-14	0	
11	B _{3u}	159	5	-	-2	-12	-1	
12	A _g	167	0	2.00×10	0	-14	-3	
13	B _{1g}	171	0	6.68	-3	-5	-5	
14	B _{3u}	173	575	-	-2	-6	-5	
15	A _g	180	0	8.37×10^{-1}	-2	-7	-9	
16	B _{1u}	184	354	-	-5	-10	-4	
17	B _{2g}	188	0	5.94×10^{-3}	0	-10	-2	
18	B _{2u}	195	362	-	-7	-7	-3	
19	A _u	211	0	-	-13	-1	-6	
20	B _{1u}	215	0	-	-12	0	-8	
21	A _g	255	0	8.71×10^{-1}	-5	0	-22	
22	B _{3u}	256	20	-	-4	0	-21	
23	A _g	265	0	9.00×10	-10	0	-22	
24	B _{2u}	267	0	-	-12	-1	-18	
25	A _u	270	0	-	-10	0	-5	
26	B _{3u}	271	0	-	-6	0	-6	
27	A _u	317	0	-	-14	0	-26	
28	B _{2u}	317	1834	-	-7	0	-17	
29	B _{3u}	327	1771	-	-14	0	-17	
30	B _{1u}	331	1451	-	-17	0	-14	
31	B _{3u}	333	21	-	-16	-3	-13	
32	B _{1u}	347	4	-	-8	0	-23	
33	B _{3g}	347	0	9.62×10^{-3}	-5	0	-21	
34	A _u	353	0	-	-8	-1	-21	
35	B _{2u}	358	8	-	-12	0	-20	
36	B _{2g}	367	0	1.52×10^{-2}	-8	-3	-22	
37	A _u	387	0	-	-20	-2	-30	
38	B _{2u}	387	3	-	-18	0	-26	
39	B _{2u}	393	3	-	-4	0	-20	
40	B _{1g}	394	0	3.33×10^{-1}	-5	-1	-16	
41	B _{1g}	408	0	7.69×10	-14	0	-25	
42	B _{1u}	410	660	-	-2	0	-26	
43	B _{3g}	415	0	6.65×10^{-1}	0	0	-17	
44	B _{2u}	437	1179	-	-10	0	-24	
45	A _g	467	0	1.18×10^2	-9	0	-41	
46	B _{3u}	468	2	-	-1	0	-27	
47	A _u	493	0	-	-5	0	-37	
48	B _{1u}	499	7	-	-4	0	-40	
49	B _{1g}	503	0	1.85	-2	0	-42	
50	B _{3u}	503	1549	-	0	0	-41	
51	B _{1u}	510	1205	-	-3	0	-41	
52	A _u	516	0	-	-8	0	-42	
53	B _{3u}	516	0	-	-3	0	-34	
54	B _{2u}	530	844	-	-1	0	-44	
55	B _{3g}	585	0	1.20×10	0	0	-51	
56	B _{2g}	589	0	9.09	0	0	-51	
57	A _g	591	0	6.34×10^{-2}	0	0	-51	
58	B _{2g}	657	0	1.91×10^{-2}	0	0	-56	
59	B _{1g}	705	0	3.26×10^{-3}	0	0	-62	
60	B _{3g}	718	0	4.01×10^{-1}				

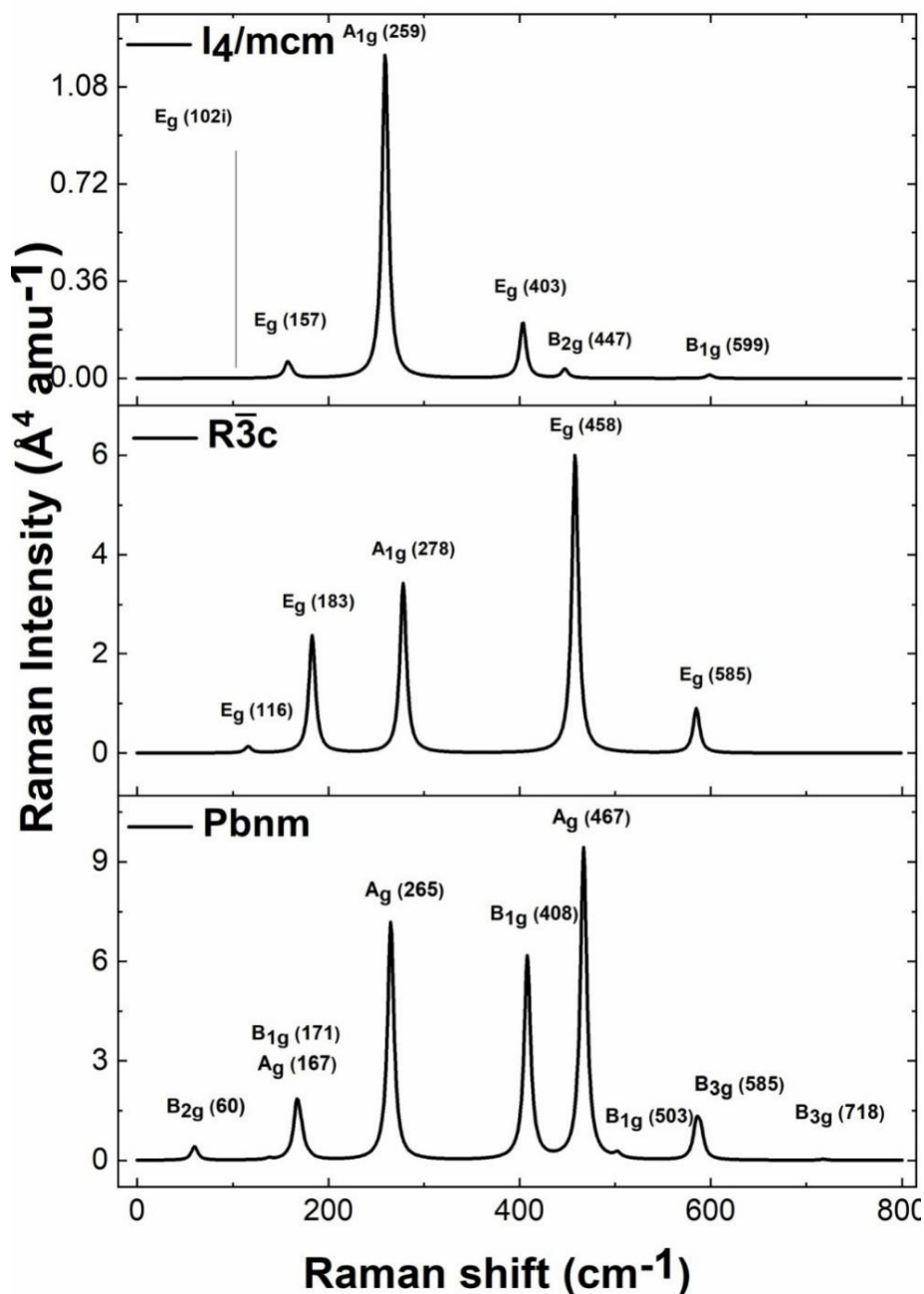


Figure 2. Raman spectrum of LaCoO_3 obtained with four different space groups of decreasing symmetry. The wavenumber and symmetry of the most relevant peaks are shown. The wavenumber, symmetry and intensity of all the modes are given in Tables 2–6.

4. Discussion and Conclusions

The evolution of the IR and Raman spectra of the LaCoO_3 perovskite along the sequence cubic-tetragonal-rhombohedral-orthorhombic has been explored. The two lowest energy structures, with space groups $R\bar{3}c$ and $Pbnm$, differ by a very small amount of energy, just 1.2 mE_h/f.u. Also the equilibrium geometries of the two are very similar (for example in the distances and angles within the octahedra). These small differences are however sufficient to differentiate in many respects the IR and Raman spectra, which could be used as complementary tools for the classification of the lowest energy structure.

Author Contributions

T.L.: Preparation, data curation, review & editing and conceptualization. R.D.: Writing-original draft, review & editing, supervision, investigation and conceptualization. M.R.: Supervision, software and validation. K.D.: Supervision, investigation. All authors have read and agreed to the published version of the manuscript.

Funding

This research received no external funding.

Institutional Review Board Statement

Not applicable.

Informed Consent Statement

Not applicable.

Data Availability Statement

Data will be made available on request.

Acknowledgments

The Direction du Numerique of the “Universite de Pau et des Pays de l’Adour” and the mesocentre Aquitain (MCIA) are acknowledged for their computing facilities.

Conflicts of Interest

The authors declare no conflict of interest.

Use of AI and AI-Assisted Technologies

No AI tools were utilized for this paper.

References

1. Glazer, A.M. The classification of tilted octahedral in perovskites. *Acta Crystallogr. Sect. B* **1972**, *28*, 3384.
2. Glazer, A.M. Simple ways of determining perovskite structures. *Acta Crystallogr. Sect. A* **1975**, *31*, 756.
3. Pascale, F.; Darco, P.; Dovesi, R. The ferromagnetic and anti-ferromagnetic phases (cubic, tetragonal, orthorhombic) of KMnF₃. A quantum mechanical investigation. *Phys. Chem. Chem. Phys.* **2021**, *23*, 26780. <https://doi.org/10.1039/D1CP03816H>.
4. El-Kelany, K.E.; Pascale, F.; Platonenko, A.; et al. Quantum mechanical simulation of various phases of KVF₃ perovskites. *J. Phys. Condens. Matter* **2022**, *34*, 285401.
5. Goldschmidt, V. Die Gesetze der Krystallochemie. *Naturwissenschaften* **1926**, *14*, 477.
6. Shannon, R.D. Revised effective ionic radii and systematic studies of interatomic distances in halides and chalcogenides. *Acta Crystallogr. Sect. A* **1976**, *32*, 751. <https://doi.org/10.1107/S0567739476001551>.
7. Dubrovin, R.M.; Garcia-Castro, A.C.; Siverin, N.V.; et al. Incipient geometric lattice instability of cubic fluoroperovskites. *Phys. Rev. B* **2021**, *104*, 144304. <https://link.aps.org/doi/10.1103/PhysRevB.104.144304>.
8. Geller, S. Crystallographic studies of perovskite-like compounds. IV Rare earth scandates, vanadites, galliates, orthochromites. *Acta Crystallogr.* **1957**, *10*, 243. <https://doi.org/10.1107/S0365110X57000778>.
9. Cwik, M.; Lorenz, T.; Baier, J.; et al. Crystal and magnetic structure of LaTiO₃: Evidence nondegenerate t_{2g} orbitals. *Phys. Rev. B* **2003**, *68*, 060401. <https://link.aps.org/doi/10.1103/PhysRevB.68.060401>.
10. Bordet, P.; Chaillout, C.; Marezio, M.; et al. Structural Aspects of the Crystallographic-Magnetic Transition in LaVO₃ around 140 K. *J. Solid State Chem.* **1993**, *106*, 253. <https://doi.org/10.1006/jssc.1993.1285>.
11. Tezuka, K.; Hinatsu, Y.; Nakamura, A.; et al. Magnetic properties of ternary sodium oxides NaLnO₂ (Ln = Rare earths). *J. Solid State Chem.* **1998**, *141*, 404. <https://doi.org/10.1016/j.jssc.2003.08.001>.
12. Li, G.; Kuang, X.; Tian, S.; et al. Structural and Conductivity of Perovskites Sr_{1-x}La_xTi_{1-x}Cr_xO₃. *J. Solid State Chem.* **2002**, *165*, 381. <https://doi.org/10.1006/jssc.2002.9561>.
13. Elemans, J.B.; Van Laar, B.; Van Der Veen, K.; et al. The crystallographic and magnetic structures of La_{1-x}Ba_xMn_{1-x}MexO₃ (Me = Mn or Ti). *J. Solid State Chem.* **1971**, *3*, 238. [https://doi.org/10.1016/0022-4596\(71\)90034-X](https://doi.org/10.1016/0022-4596(71)90034-X).
14. Dann, S.; Currie, D.; Weller, M.; et al. The synthesis and structures of Sr₂FeO₄. *J. Solid State Chem.* **1994**, *109*, 134. [https://doi.org/10.1016/0022-4596\(91\)90263-H](https://doi.org/10.1016/0022-4596(91)90263-H).
15. Thornton, G.; Toled, B.; Hewat, A. A neutron diffraction study of LaCoO₃ on the temperature range 42 < T < 1248 K. *J. Solid State Chem.* **1986**, *61*, 301. [https://doi.org/10.1016/0022-4596\(86\)90035-6](https://doi.org/10.1016/0022-4596(86)90035-6).
16. Haas, O.; Struis, R.; McBreen, J. Synchrotron X-ray absorption of LaCoO₃ perovskite. *J. Solid State Chem.* **2004**, *177*, 1000. <https://doi.org/10.1016/j.jssc.2003.10.004>.

17. Garca-Munoz, J.L.; Rodriguez-Carvajal, J.; Lacorre, P.; et al. Neutron-diffraction study of RNiO₃ (R = La, Pr, Nd, Sm) Electronically induced structural changes across the metal-insulator transition. *Phys. Rev. B* **1992**, *46*, 4414. <https://doi.org/10.1103/PhysRevB.46.4414>.
18. Bringley, J.F.; Scott, B.A.; La Placa, S.J.; et al. Structural and properties of the LaCuO_{3-δ} perovskites. *Phys. Rev. B* **1993**, *47*, 15269. <https://doi.org/10.1103/PhysRevB.47.15269>.
19. Darracq, S.; Matar, S.; Demazeau, G. Correlations between the structural distortion of LaCuO₃ lattice and the resulting physical properties. *Solid State Commun.* **1993**, *85*, 961. [https://doi.org/10.1016/0038-1098\(93\)90713-W](https://doi.org/10.1016/0038-1098(93)90713-W).
20. Currie, D.B.; Weller, M.T. Structure of LaCuO₃ by powder neutron diffraction. *Acta Crystallogr. C* **1991**, *47*, 696. <https://doi.org/10.1107/S010827019001040X>.
21. Becke, A.D. Density-functional thermochemistry. III. The role of exact exchange. *J. Chem. Phys.* **1993**, *98*, 5648.
22. Lee, C.; Yang, W.; Parr, R. Development of the Colle-Salvetti correlation-energy formula into a functional of the electron density. *Phys. Rev. B* **1988**, *37*, 785.
23. Dovesi, R.; Saunders, V.R.; Roetti, C.; et al. Quantum-mechanical condensed matter simulations with CRYSTAL. In *CRYSTAL Users Manual*; Universita di Torino: Torino, Italy, 2017.
24. Dovesi, R.; Pascale, F.; Civalieri, B.; et al. The CRYSTAL code, 1976-2020 and beyond, a long story. *J. Chem. Phys.* **2020**, *152*, 204111.
25. Dovesi, R.; Pisani, C.; Roetti, C.; et al. Treatment of Coulomb interactions in Hartree-Fock calculations of periodic systems. *Phys. Rev. B* **1983**, *28*, 5781. <https://doi.org/10.1103/PhysRevB.28.5781>.
26. Causà, M.; Dovesi, R.; Orlando, R.; et al. Treatment of the exchange interactions in Hartree-Fock LCAO calculations of periodic systems. *J. Phys. Chem.* **1988**, *92*, 909. <https://doi.org/10.1021/j100315a010>.
27. Dovesi, R.; Saunders, V.R.; Roetti, C.; et al. *CRYSTAL06 Users Manual*; Universita di Torino: Torino, Italy, 2006.
28. Pascale, F.; Zicovich-Wilson, C.M.; Gejo, F.L.; et al. The calculation of the vibrational frequencies of crystalline compounds and its implementation in the CRYSTAL code. *J. Comput. Chem.* **2004**, *25*, 888. <https://doi.org/10.1002/jcc.20019>.
29. Zicovich-Wilson, C.M.; Pascale, F.; Roetti, C.; et al. Calculation of the vibration frequencies of alpha-quartz: The effect of Hamiltonian and basis set. *J. Comput. Chem.* **2004**, *25*, 1873. <https://doi.org/10.1002/jcc.20120>.
30. Carteret, C.; Pierre, M.D.L.; Dossot, M.; et al. The vibrational spectrum of CaCO₃ aragonite: A combined experimental and quantum-mechanical investigation. *J. Chem. Phys.* **2013**, *138*, 014201.
31. Ferrero, M.; Rerat, M.; Kirtman, B.; et al. Calculation of first and second static hyperpolarizabilities of one- to three-dimensional periodic compounds. Implementation in the CRYSTAL code. *J. Chem. Phys.* **2008**, *129*, 244110. <https://doi.org/10.1063/1.3043366>.
32. Ferrero, M.; Rerat, M.; Orlando, R.; et al. Coupled perturbed Hartree-Fock for periodic systems: The role of symmetry and related computational aspects. *J. Chem. Phys.* **2008**, *128*, 014110.
33. Maschio, L.; Kirtman, B.; Rerat, M.; et al. Ab initio analytical Raman intensities for periodic systems through a coupled perturbed Hartree-Fock-Kohn-Sham method in an atomic orbital basis. II. Validation and comparison with experiments. *J. Chem. Phys.* **2013**, *139*, 164102. <https://doi.org/10.1063/1.4824443>.
34. El-Kelany, K.E.; Platonenko, A.; Doll, K.; et al. The Structural, Electronic and vibrational Properties of LaCrO₃. A Quantum Mechanical Investigation by using an All Electron Gaussian Type Basis Set and a Full Range Hybrid Functional. *J. Comput. Chem.* **2025**, *46*, e27523. <https://doi.org/10.1002/jcc.27523>.
35. El-Kelany, K.E.; Platonenko, A.; Sambrano, J.; et al. The charge and spin density of five LBO₃ perovskites (B= Sc, Ti, V, Cr and Co). A Mulliken analysis. *Chem. Phys.* **2025**, *591*, 112594. <https://doi.org/10.1016/j.chemphys.2024.112594>.